Supporting information. Effect of water loading on the stability of pristine and defected UiO-66

E. Acuna-Yeomans,[†,‡] P. J. Goosen,[¶] J. J. Gutierrez-Sevillano,[*,§] D. Dubbeldam,[‖] and S. Calero[*,†,‡]

†*Materials Simulation and Modelling, Department of Applied Physics and Science Education, Eindhoven University of Technology, 5600 MB Eindhoven, The Netherlands*

‡*Eindhoven Institute for Renewable Energy Systems (EIRES), Eindhoven University of Technology, P.O. Box 513, 5600 MB Eindhoven, The Netherlands*

¶*Eindhoven University of Technology, Eindhoven, Netherlands*

§*Center for Nanoscience and Sustainable Technologies (CNATS), Universidad Pablo de Olavide, 41013 Seville, Spain*

‖*Van 't Hoff Institute for Molecular Sciences, University of Amsterdam, Amsterdam, Netherlands*

E-mail: jjgutierrez@upo.es; s.calero@tue.nl

Additional information on the framework force fields and structures

In this study, the pristine and defected UiO-66 frameworks were modeled using the family of periodic force fields developed by Rogge et al. These force fields are designed to accurately represent both covalent and noncovalent interactions within the framework, ensuring reliable predictions of the structural and mechanical properties of the frameworks. The construction of these force fields follows the QuickFF procedure, as described by Rogge et al.[1] The force fields are composed of two main contributions:

- **Covalent Terms:** These terms model the chemical bonds within the framework using internal coordinates such as bond lengths, bend angles, dihedral angles, torsions, and out-of-plane distances. These terms are fitted to first-principles data derived from representative cluster model systems.

- **Noncovalent Terms:** These model the long-range interactions between nonbonded atoms, consisting of electrostatic interactions (EI) and van der Waals (vdW) forces. The electrostatic interactions are described by Coulomb interactions between spherical Gaussian densities, with charges derived from the DFT electron density of each cluster model. The van der Waals interactions are modeled using a two-parameter MM3 Buckingham potential.

To generate these force fields, they isolated cluster models were first extracted from DFT-optimized periodic structures. These isolated models were then optimized using DFT with the B3LYP functional, and the geometry, Hessian, and electron density were used as input to the QuickFF procedure to estimate the force field parameters. For each of the pristine and defected UiO-66 structures, a separate periodic force field was constructed by combining the parameters derived from the relevant isolated cluster models.

The force fields developed by Rogge et al. were employed to model both the pristine and defected UiO-66 structures in this study. The structures themselves were generated using the unit cell crystallographic information file (CIF) constructed by D. Dubbeldam (included

as part of the RASPA[2] simulation package), which was based on previously reported experimental measurements by J. S. Cavka et al.[3] To prepare the input topologies for LAMMPS, 2x2x2 representations of the periodic unit cells were created using an in-house script. This script utilized the atomic positions from the same CIF file and the framework atom connectivity information inferred from each specific force field. Figure 1 visually depicts these structures, with the missing linkers clearly indicated to facilitate understanding of the defect sites.

- **Type 0 structure:** Two of the four inorganic clusters are 11-fold coordinated. Average coordination number of 11.5.
- **Type 1 structure:** Two of the four inorganic clusters are 11-fold coordinated, one is 10-fold coordinated, and one is 12-fold coordinated. Average coordination number of 11.
- **Type 2 structure:** Two of the four inorganic clusters are 10-fold coordinated. Average coordination number of 11.
- **Type 3 structure:** All four inorganic clusters are 11-fold coordinated. Average coordination number of 11.
- **Type 4 structure:** Two of the four inorganic clusters are 11-fold coordinated, one is 10-fold coordinated, and one is 12-fold coordinated. Average coordination number of 11.
- **Type 5 structure:** All four inorganic clusters are 11-fold coordinated. Average coordination number of 11.
- **Type 6 structure:** Two of the four inorganic clusters are 10-fold coordinated. Average coordination number of 11.
- **Type 7 structure:** All four inorganic clusters are 11-fold coordinated. Average coordination number of 11.

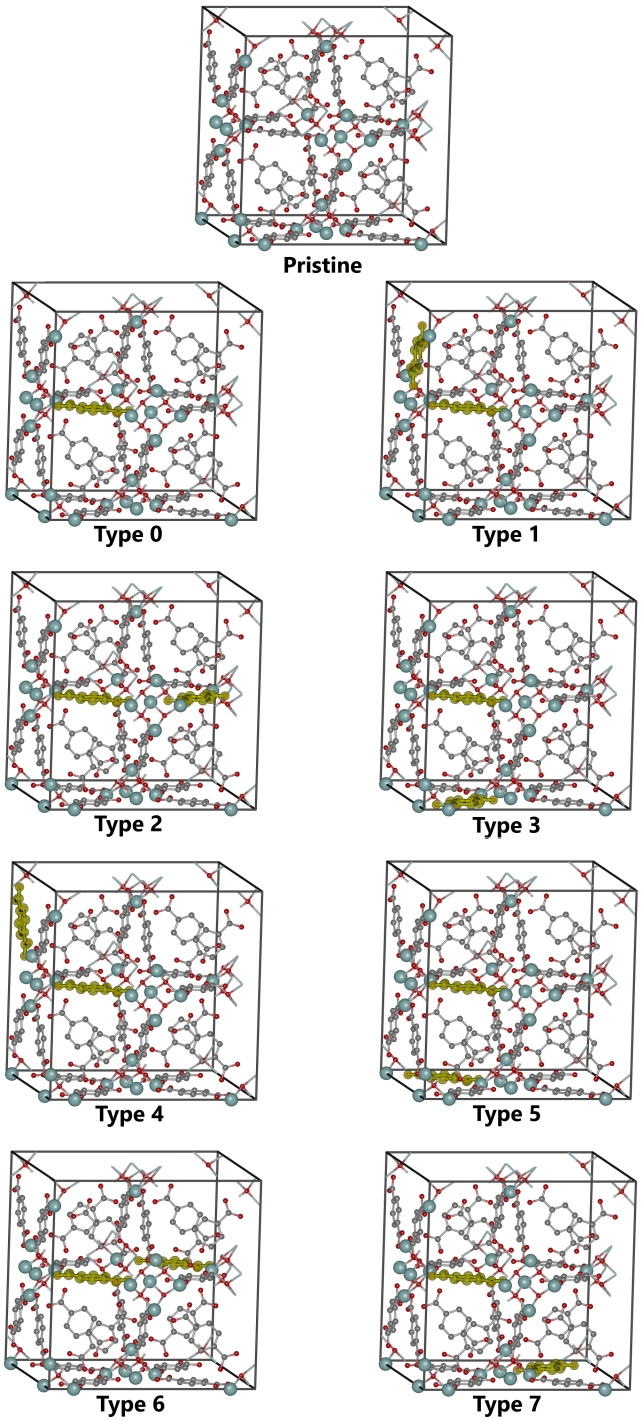

Figure 1: Periodic unit cell representations of the structures considered in this work. Highligted in yellow are the missing BDC organic in each structure. In the pictures, the linker hydrogen atoms and linker-cluster bonds were removed for clarity. All type 1-7 defected structures share one of the removed linker from the type 0 parent.

Complementary figures on the effect of water loading on the pristine structures

This section provides additional figures and plots that complement the first part of the Results section in the main text. The radial distribution functions (RDFs) between water oxygen atoms (O_{H_2O}) and potential bonding sites in the pristine framework at higher water loadings of 40 and 100 water molecules per unit cell are shown in Figure 2. Figure 3 presents volumetric density maps illustrating that hybrid mixing captures the formation of one-dimensional water chains and clusters, which emerge as the loading increases, causing more water molecules to shift from the zirconium clusters toward the central regions of the pores. Figure 4 compares the mean square displacement (MSD) of water molecules for the two interaction methods at a moderate loading of 40 water molecules per unit cell. The differences in MSD between the two methods highlight the impact of the mixing approach on water mobility within the pores of UiO-66. Finally, Figure 5 includes additional plots showing the average bond length changes for non-preferential adsorption sites, Zr-Ox and Zr-Oh, upon water loading.

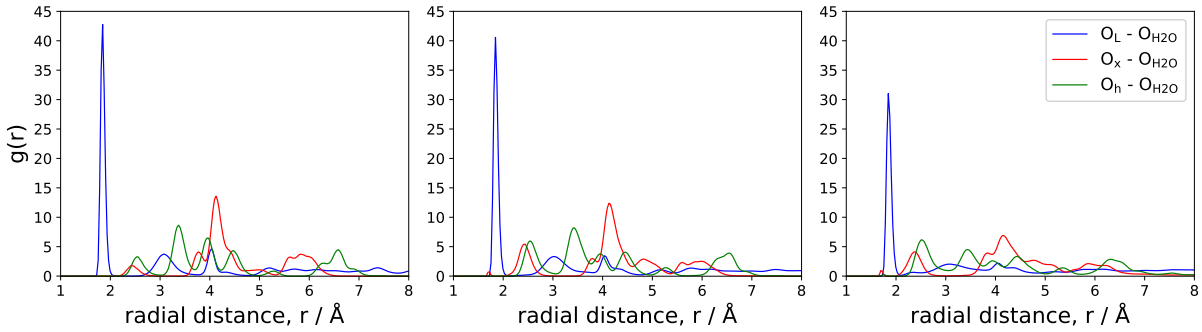

(a)

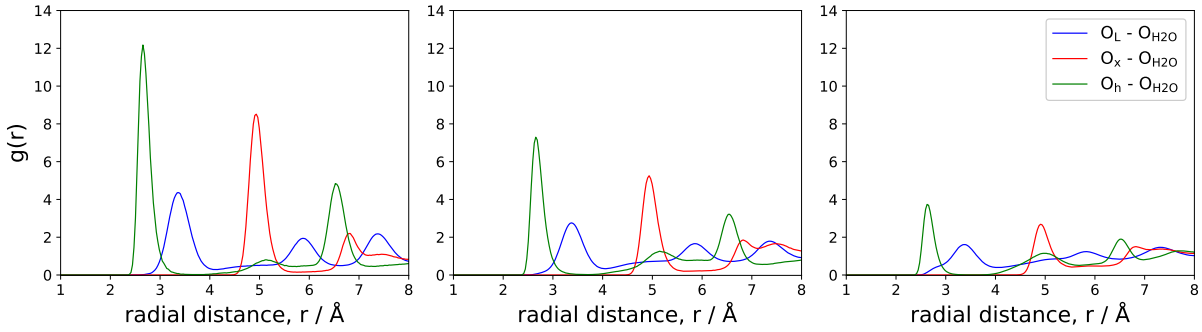

(b)

Figure 2: RDFs between water oxygens and potential interaction sites around the inorganic cluster at loadings of 10, 40 and 100 molecules per unit cell (from left to right), using (a) L-B mixing (b) hybrid mixing. Computed at a temperature and pressure of 300 K and 1 atm, respectively.

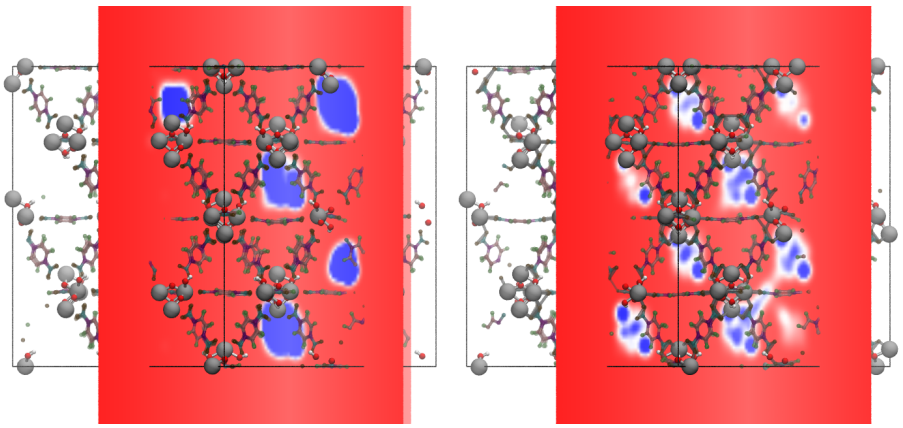

(a) (b)

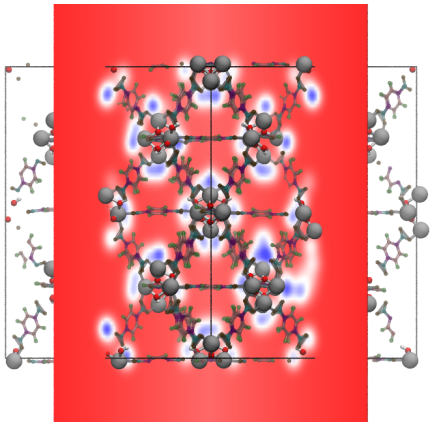

(c)

Figure 3: Volumetric density maps of water over a trajectory of 500 ps for a loading of (a) 10 and (b) 40 molecules per unit cell using hybrid mixing. Higher density of water molecules presented in blue and lower density in red. Using hybrid mixing, at low loadings the molecules occupy pore space near the main interaction sites and hopping from one to another within the same pore is observed. Movement between pores observed at moderate and higher loadings. Subfigure (c) shows a volumetric density map of water at a loading of 10 molecules per unit cell using L-B mixing.

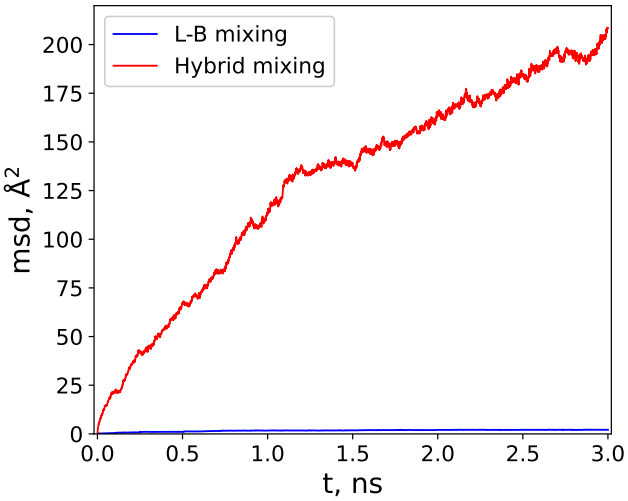

Figure 4: MSD of water molecules over a simulation period of 3 nanoseconds at a loading of 40 molecules per unit cell at atmospheric conditions. L-B mixing simulations (blue curve) predicts minimal increase in MSD, indicative of heavily restricted molecular mobility within the framework. In contrast, hybrid mixing simulations (red curve) predict a more realistic diffusive behavior.

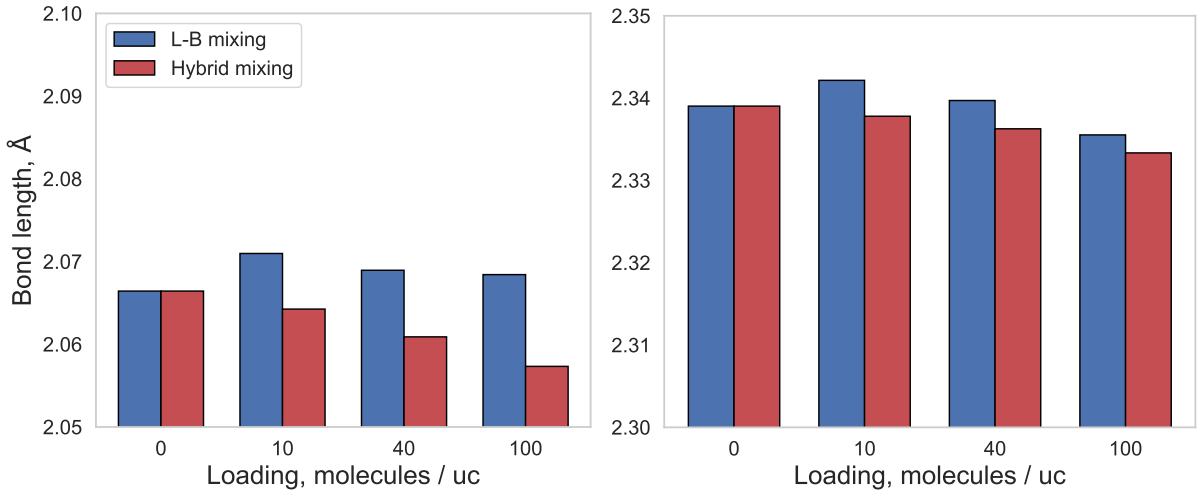

(a) (b)

Figure 5: Sverage bond length between (a) Zr and O_{Ox} and between (b) Zr and O_{Oh}. The pictured bars in (a) and (b) at a particular loading value are the result of the same four sets of simulations pictured in Figure 2 of the main text.

Complementary figures on the effect of water loading on the defected structures

This section provides additional figures and plots that complement the second part of the Results section in the main text. Predicted amorphization pressure for all defected structures are presented in Figure 6. RDFs between water molecules and the zirconium atoms for the structure containing linker vacancies (and containing uncoordinated Zr atoms) are provided in Figures 7-12. Direct mixing methodology comparison of system volume changes upon water loading are presented in Figures 13-15, where the results for representative pristine, 1-missing linker and 2-missing linker structures are shown.

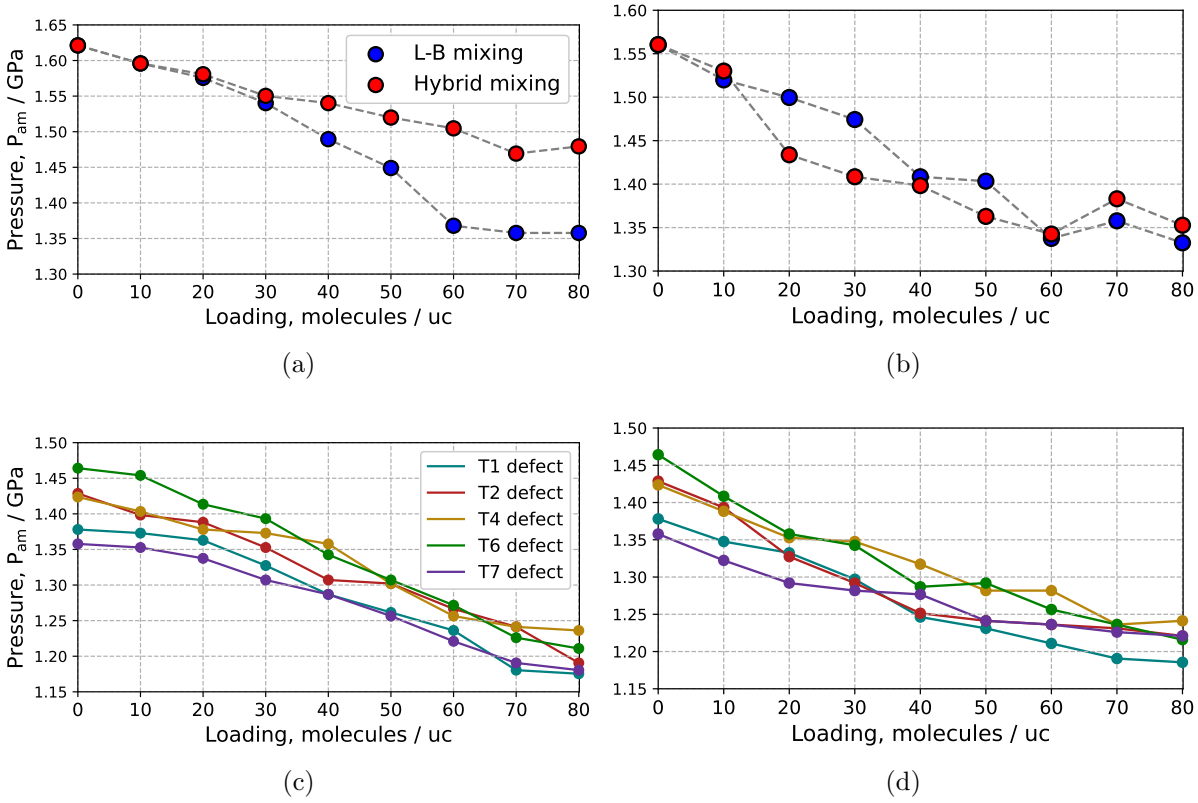

Figure 6: A closer look at the P_{am} trends predicted using both mixing models. (a) Comparison for the structure with average inorganic cluster coordination of 11.5. (b) Comparison for the most stable 11-coordinated structure (type 3). (c) and (d) present a breakdown of the remaining structures with 11.0 cluster coordination for the L-B and hybrid method, respectively. Hybrid mixing simulations predict a sharper decrease in P_{am} values at low loadings when compared to the L-B mixing results. Both methods predict comparable high-loading values for all structures with two linker vacancies per unit cell.

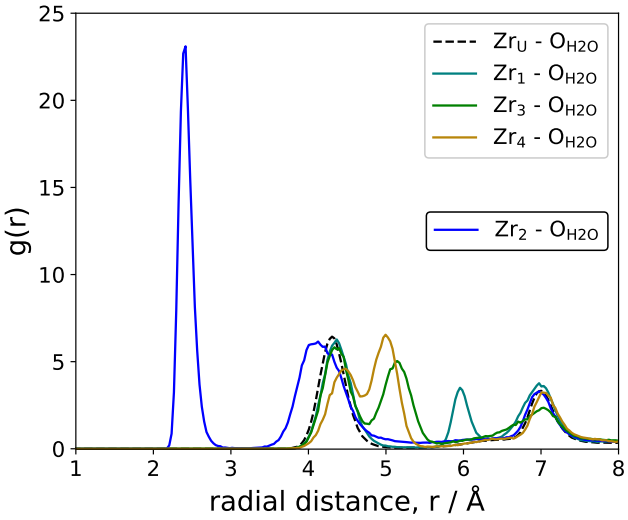

Figure 7: RDF between water molecules and the zirconium atoms for the defected type 0 structure. Grey legend indicates fully coordinated (8) zirconium atoms and black legend indicates Zr atoms with lower coordination. The blue curve depicts the RDF between H_2O and the 7-coordinated Zr_2 site.

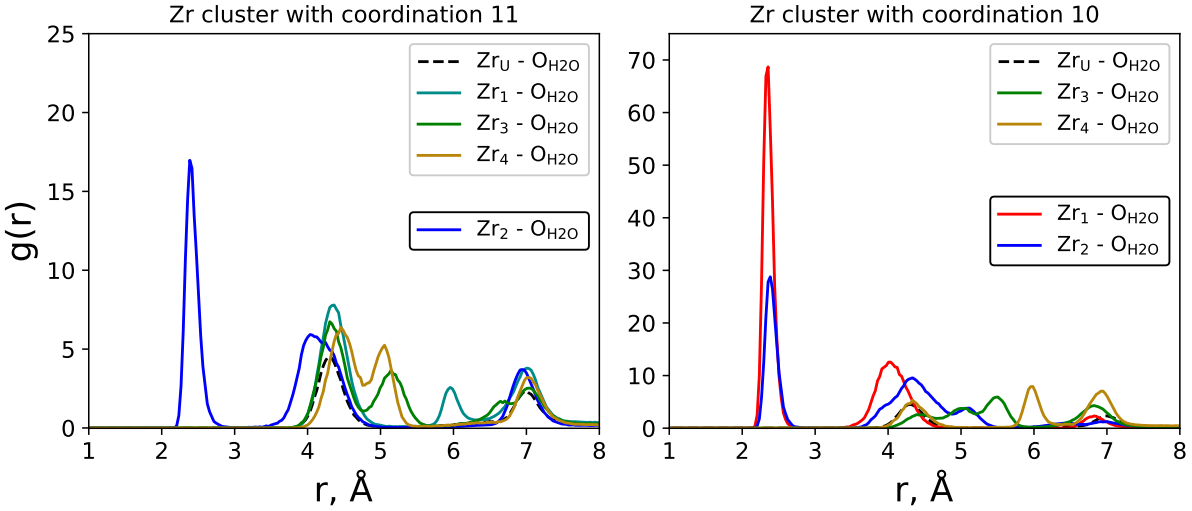

Figure 8: RDF between water molecules and the zirconium atoms for the defected type 1 structure. Grey legend indicates fully coordinated (8) zirconium atoms and black legend indicates Zr atoms with lower coordination. The blue curves depict the RDF between H_2O and 7-coordinated Zr_2 sites. The red curve depicts the RDF between H_2O and the 6-coordinated Zr_1 site.

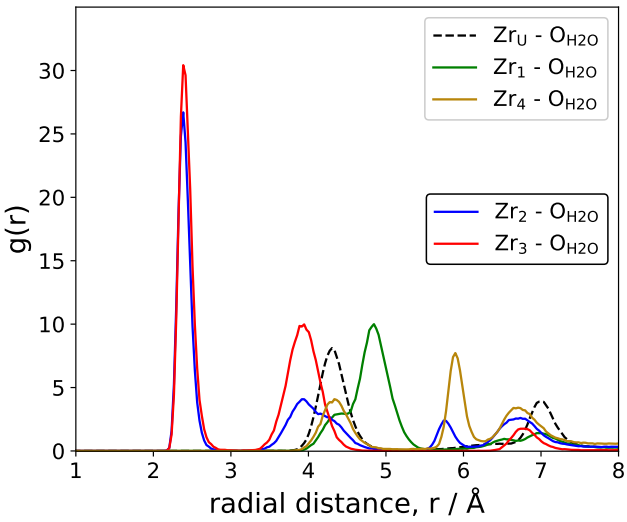

Figure 9: RDF between water molecules and the zirconium atoms for the defected type 2 structure. Grey legend indicates fully coordinated (8) zirconium atoms and black legend indicates Zr atoms with lower coordination. The blue curve depicts the RDF between H_2O and the 7-coordinated Zr_2 site. The red curve depicts the RDF between H_2O and the 6-coordinated Zr_3 site.

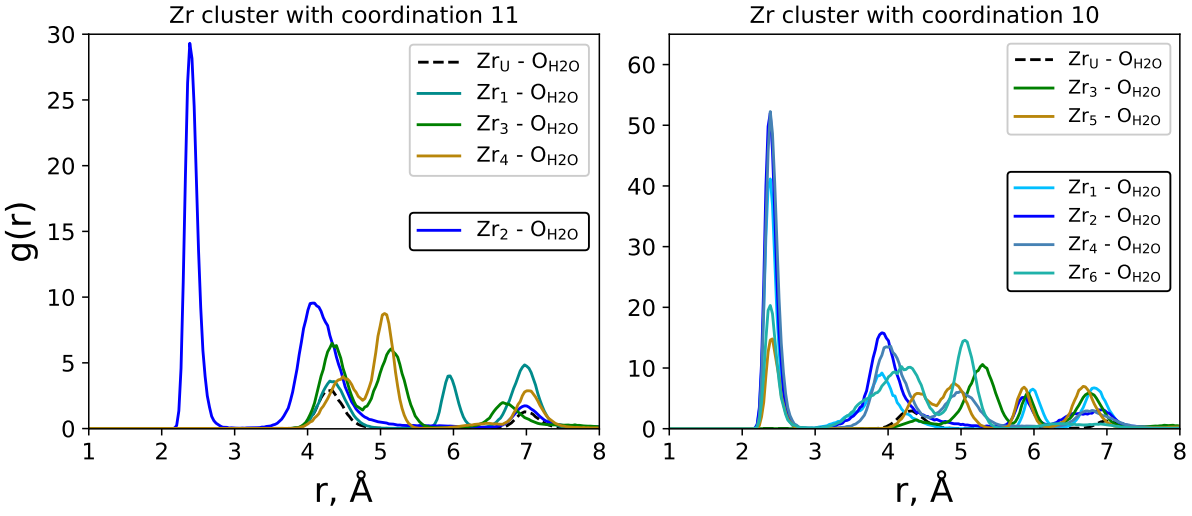

Figure 10: RDF between water molecules and the zirconium atoms for the defected type 4 structure. Grey legend indicates fully coordinated (8) zirconium atoms and black legend indicates Zr atoms with lower coordination. The blue-colored curves depict the RDF between H_2O and 7-coordinated sites.

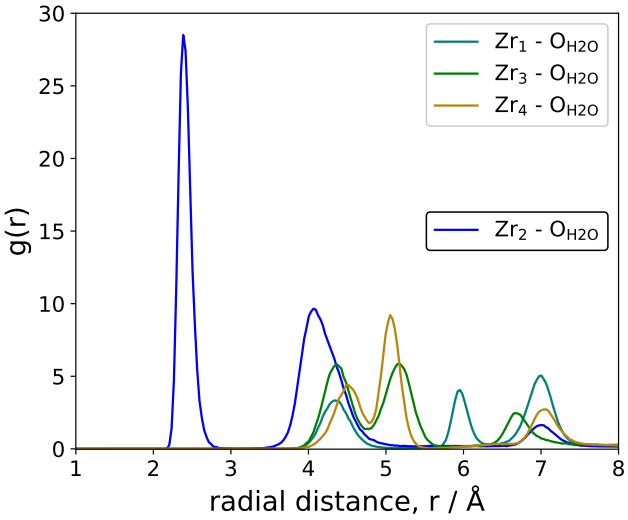

Figure 11: RDF between water molecules and the zirconium atoms for the defected type 5 structure. Grey legend indicates fully coordinated (8) zirconium atoms and black legend indicates Zr atoms with lower coordination. The blue curve depicts the RDF between H_2O and the 7-coordinated Zr_2 site.

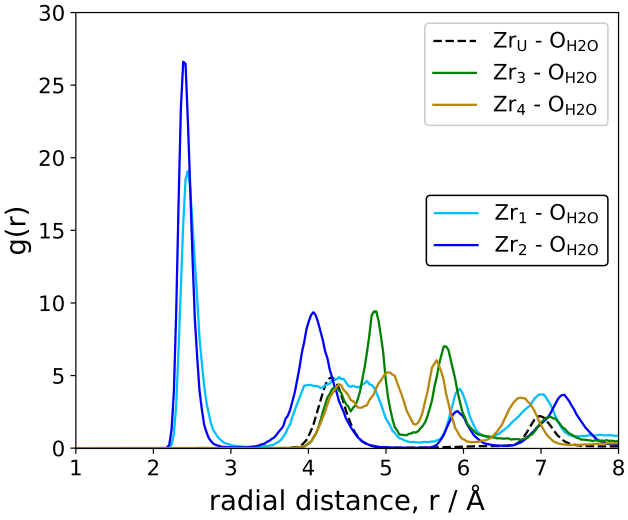

Figure 12: RDF between water molecules and the zirconium atoms for the defected type 2 structure. Grey legend indicates fully coordinated (8) zirconium atoms and black legend indicates Zr atoms with lower coordination. The blue-colored curves depict the RDF between H_2O and 7-coordinated sites.

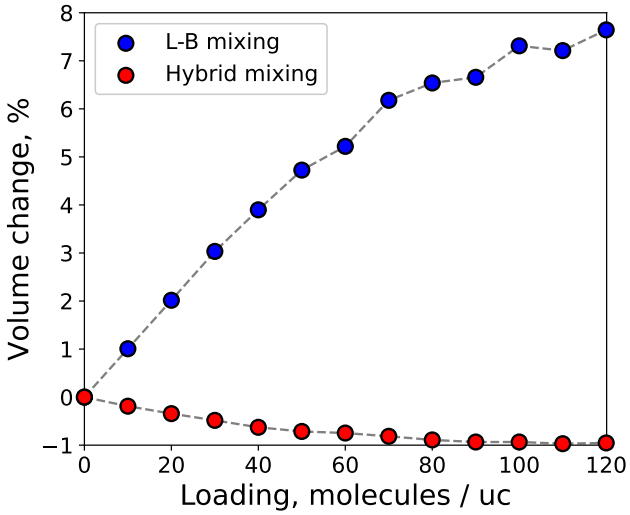

Figure 13: Comparison of percentage volume change as a function of loading at atmospheric conditions for the pristine structure.

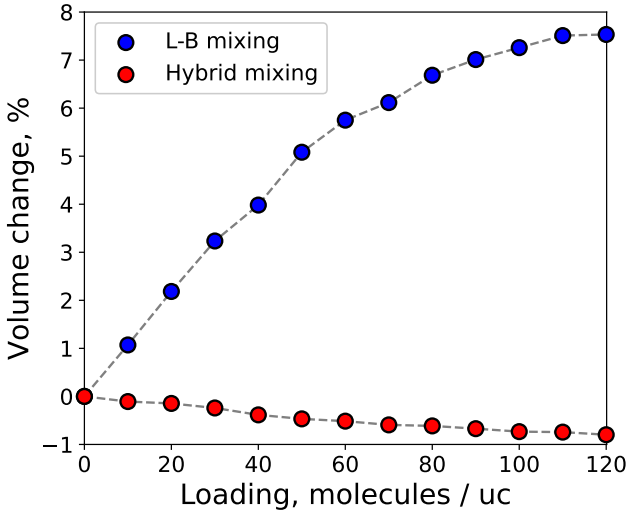

Figure 14: Comparison of percentage volume change as a function of loading at atmospheric conditions for the structure with one linker vacancy per unit cell (type 0 structure).

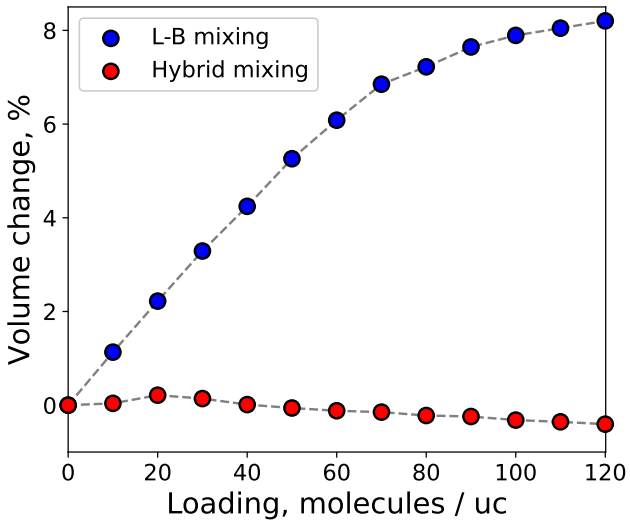

Figure 15: Comparison of percentage volume change as a function of loading at atmospheric conditions for a structure with two linker vacancies per unit cell (type 3 structure).

Framework collapse

Regarding the mechanism of collapse, although the implemented force fields are classical and do not allow for bond creation or breaking, a well tuned FF can help in characterizing the elasticity of the material, identifying the nature of instability at high pressures as well as characterizing the movement of certain regions prior to collapse. Regardless of the mixing model used, the intra-framework force field predicts collapse due to spatially alternated rotations of the zirconium clusters and a corresponding loss of planarity of organic linkers, as can be seen in Fig. 16.

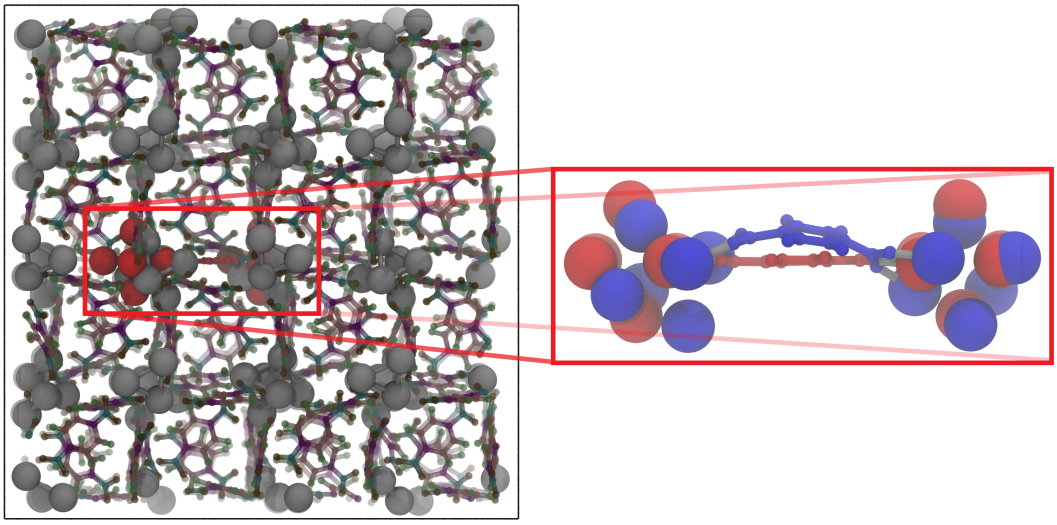

Figure 16: XY snapshot of the pristine framework atoms after amorphization has occurred. The positions of two zirconium clusters and their connecting linker are highlighted and colored according to average atomic positions before (red) and after (blue) amorphization.

References

(1) Rogge, S. M. J.; Wieme, J.; Vanduyfhuys, L.; Vandenbrande, S.; Maurin, G.; Verstraelen, T.; Waroquier, M.; Van Speybroeck, V. Thermodynamic Insight in the High-Pressure Behavior of UiO-66: Effect of Linker Defects and Linker Expansion. *Chemistry of Materials* **2016**, *28*, 5721–5732.

(2) Dubbeldam, D.; Calero, S.; Ellis, D. E.; Snurr, R. Q. RASPA: molecular simulation software for adsorption and diffusion in flexible nanoporous materials. *Mol. Simul.* **2016**, *42*, 81–101.

(3) Cavka, J. H.; Jakobsen, S.; Olsbye, U.; Guillou, N.; Lamberti, C.; Bordiga, S.; Lillerud, K. P. A New Zirconium Inorganic Building Brick Forming Metal Organic Frameworks with Exceptional Stability. *Journal of the American Chemical Society* **2008**, *130*, 13850–13851.